2024 European Control Conference (ECC)
June 25-28, 2024. Stockholm, Sweden

State Estimation for a Tractor Semi-trailer System using a Minimum-Energy Filter

Damiano Rigo, Alessandro Saccon, Mohsen Alirezaei, Erjen Lefeber, Nicola Sansonetto and Riccardo Muradore

***Abstract*— In this article we apply a second-order minimum-energy filter based on Lie groups to the problem of parking a truck with a semi-trailer in a docking station. The use of the filter, that exploits the geometry of Lie groups to estimate the truck and trailer pose, is useful to improve the precision of the state and thus perform better controls. We consider two different types of measurements: the first consists of GPS-like devices that detect the positions of the front wheels of the truck and the rear wheels of the trailer, and the second improves the measurement of the rear wheels with the measurement of the pose of the trailer with a LIDAR sensor. The accuracy of the LIDAR is useful for having a better estimate when parking in reverse. We show two simulations with two different datasets.**

I. INTRODUCTION

The problem of tracking and control of vehicles has received a lot of attention in recent years due to its real-life applications. Among all the problems that can be examined, particular attention has to be devoted to the study of the control of articulated vehicles ([1], [2], [3]). One difficulty that arises in these approaches is the fact that they are not described by rigid bodies equations (since they present pivot points), and thus the dynamics and controls get complicated. Moreover, the systems become unstable when the vehicles move to reverse, and this can give rise to the jackknifing problem. These problems become more evident in parking maneuvers. The issue of autonomous or guided parking, facilitated through the measurement of the external environment or the knowledge of one's own state, has been developed in many areas (see e.g. [4]). One of the most used systems for detecting positions is the GPS, whose use has been growing since the 1990s ([5]). Another application that has had major developments in recent years is autonomous parking with the use of LIDAR sensors ([6], [7]). Unfortunately, even if these sensors can be very precise, in real-life applications the accuracy of the measurements are not perfect due to disturbances and noises. Moreover, they cannot directly provide information about other components of the state space. In order to overcome these problems, a filter can be introduced. The literature presents many types of different filters. The most famous are the Kalman filter and its variants ([8], [9], [10]). In [11] the authors, starting from an idea presented in [12], propose a second-order optimal filter constructed on Lie groups. This filter has the advantage of not having to take into account any assumptions on the nature of the errors and the possibility of considering nonlinear dynamics. Moreover, it exploits the symmetries in the state space of the system to produce good estimations. An application of this theorem for a free rigid body case can be found in [13], an implementation to a nonholonomic case is provided in [14], while a comparison with the extended Kalman filter is given in [15].

In this paper we propose an approach to overcome the problem of having good state estimates for a truck semi-trailer system in a parking maneuver. We present an application of the second-order optimal filter applied to a scale

(a) Truck and semi-trailer in a real parking area.

(b) Truck and semi-trailer model in Automotive lab.

This work has been partially supported by the project of the Italian Ministry of Education, University and Research (MIUR) "Dipartimenti di Eccellenza 2018-2022" and "GNFM-INDAM".

Damiano Rigo and Riccardo Muradore are with the Department of Engineering for Innovation Medicine, University of Verona, 37134, Italy
damiano.rigo@univr.it
riccardo.muradore@univr.it
Alessandro Saccon, Mohsen Alirezaei and Erjen Lefeber are with the Department of Mechanical Engineering, Eindhoven University of Technology, Eindhoven, Netherlands
a.saccon@tue.nl
m.alirezaei@tue.nl
a.a.j.lefeber@tue.nl
Nicola Sansonetto is with the Department of Computer Science, University of Verona, 37134, Italy
nicola.sansonetto@univr.it

model. The measured trajectories are obtained by adding noises to the poses provided by a motion capture optical system to reproduce a real-case scenario. We simulate the cases where different devices are available or not: in the first part of the maneuver, when the system is far from the docking station, only GPS antennas are available; in the second part, when the system is moving in reverse close to the station, a LIDAR sensor is added.

The rest of the article is organized as follows. In Section II we recall the kinematics of a truck semi-trailer system. In Section III we report the second-order optimal minimum energy filter structure. Section IV is devoted to the derivation of the geometric structure that underlies the kinematics. In Section V and VI we describe the laboratory setting and provide the results of the simulations, respectively, while conclusions are presented in Section VII.

II. KINEMATICS

The system under study is an articulated vehicle composed of a leading truck and a semi-trailer (Fig. 2). We consider an inertial frame of reference $\Sigma_i = \{e_x^i, e_y^i\}$ attached to the docking station with the origin in the final target, and a right-handed body frame $\Sigma_b = \{e_1^b, e_2^b\}$ on the truck, centered in the position of the midpoint of the rear axle (x,y).

The configuration space of the truck is SE(2) with coordinates (x,y,α) with respect to the inertial frame, where α is the angle that the truck forms with the inertial frame. At distance ℓ_1 from (x,y), the pair (x_0,y_0) represents the midpoint of the front axle.

Also the configuration space of the trailer is given by SE(2) with coordinates (x_2,y_2,β). The pair (x_2,y_2) represents the position of the midpoint of the rear axle and β is the angle with respect to the inertial frame. The semi-trailer is hooked to the truck through an articulation point (x_{1_c},y_{1_c}) at distance (ℓ_{1_c}) from (x,y), while ℓ_2 is the distance between (x_2,y_2) and the articulation point. These points are related by

$$\begin{aligned} x_0 &= x+\ell_1\cos\alpha,\\ y_0 &= y+\ell_1\sin\alpha,\\ x_{1_c} &= x+\ell_{1_c}\cos\alpha,\\ y_{1_c} &= y+\ell_{1_c}\sin\alpha,\\ x_2 &= x_{1_c}-\ell_2\cos\beta,\\ y_2 &= y_{1_c}-\ell_2\sin\beta. \end{aligned}$$

The configuration space is given by $\mathrm{SE}(2)\times\mathrm{SO}(2)$, where SE(2) denotes the pose of the truck and SO(2) the angle β.

The truck and the semi-trailer are modelled as rigid bodies with nonholonomic constraints given by:

$$\begin{aligned} \dot{x}\sin\alpha-\dot{y}\cos\alpha &= 0,\\ \dot{x}_2\sin\beta-\dot{y}_2\cos\beta &= 0, \end{aligned}$$

that do not allow orthogonal components of the velocities. The lateral velocity of the front wheel, expressed in the chassis frame, is equal to $V_1\tan\delta$, where V_1 is the vehicle forward velocity at the rear axle and δ is the front wheel steering angle.

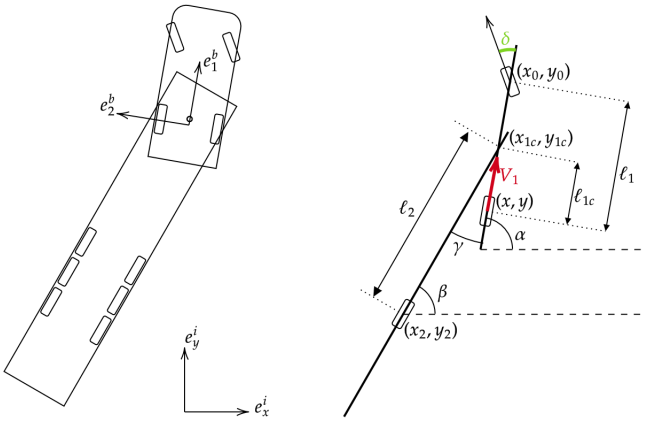

Fig. 2: Scheme of truck semi-trailer model.

The equations of motion for the truck semi-trailer system are then given by

$$\begin{cases} \dot{x} &= V_1\cos\alpha\\ \dot{y} &= V_1\sin\alpha\\ \dot{\alpha} &= \frac{1}{\ell_1}V_1\tan\delta\\ \dot{\beta} &= \frac{1}{\ell_2}\left(V_1\sin\gamma_1-\dot{\alpha}\ell_{1c}\cos\gamma_1\right), \end{cases} \tag{1}$$

where $\gamma_1=\alpha-\beta$ is the angle between the truck and the trailer. The lateral velocity of the attachment point (x_{1_c},y_{1_c}) is equal to $V_2\tan\alpha$, where $V_2=V_1\cos\gamma_1-\dot{\alpha}\ell_{1_c}\sin\gamma_1$ is the velocity at the rear axle of the trailer.

III. FILTER

In this section we recall the second-order optimal filter constructed on Lie groups described in [11]. We assume the reader is familiar with the terminology of differential geometry and Lie groups theory (see e.g. [16], [17], [18]).

We denote with G the Lie group that underlies the dynamics, and with $\mathfrak{g}$ its Lie algebra. The dynamics of our vehicle is described by the following deterministic system:

$$\dot{g}(t)=g(t)\big(\lambda(g(t),u(t),t)+B\xi(t)\big),\quad g(t_0)=g_0, \tag{2}$$

where $g(t)\in G$ is the state, $u(t)\in\mathbb{R}^m$ is the external input, $\xi(t)$ is the unknown model error, $\lambda: G\times\mathbb{R}^m\times\mathbb{R}\to\mathfrak{g}$ the left trivialized dynamics and $B:\mathbb{R}^d\to\mathfrak{g}$ a linear map.

The knowledge of the system with respect to the environment comes through some sensors and tools, and is modelled with a measurement equation given by:

$$y(t)=h(g(t),t)+D\varepsilon(t), \tag{3}$$

where $h: G\times\mathbb{R}\to\mathbb{R}^p$ is the output map, $\varepsilon\in\mathbb{R}^p$ is the unknown measurement error and $D:\mathbb{R}^p\to\mathbb{R}^p$ is an invertible linear map.

Given the external command $u(t)$ and the measurement output $y(t)$, the goal of the filter is to find the best estimate of the state $g(\cdot)$ minimizing the cost functional

$$J(\xi,\varepsilon,g_0,t,t_0):=m(g_0,t,t_0)+\int_{t_0}^{t}l(\xi(\tau),\varepsilon(\tau),t,\tau)\mathrm{d}\tau, \tag{4}$$

where $l : \mathbb{R}^d \times \mathbb{R}^p \times \mathbb{R} \times \mathbb{R} \to \mathbb{R}$ is the incremental cost defined by

$$l(\xi, \varepsilon, t, \tau) := 1/2 e^{-c(t-\tau)}(\mathscr{R}(\xi) + \mathscr{Q}(\varepsilon)), \tag{5}$$

with c a non-negative scalar and

$$\mathscr{R} : \mathbb{R}^d \to \mathbb{R}, \quad \mathscr{Q} : \mathbb{R}^p \to \mathbb{R},$$

two quadratic forms that weigh the contribution of model and measurement errors. The function $m : G \times \mathbb{R} \times \mathbb{R} \to \mathbb{R}$ is the initial cost and takes the form

$$m(g_0, t, t_0) := 1/2 e^{-c(t-t_0)} m_0(g_0), \tag{6}$$

with $m_0 : G \to \mathbb{R}$ a bounded smooth function.

We recall now the main result in [11]:

Lemma 1: ([11, Theorem 4.1]) Consider the system defined by (2) and (3) with the energy cost functional (4)-(6). Then the second-order-optimal minimum-energy filter yields the estimation state $\widehat{g}$ given by

$$\widehat{g}^{-1}\dot{\widehat{g}} = \lambda_t(\widehat{g}, u) + K(t) r_t(\widehat{g}), \quad \widehat{g}(t_0) = \widehat{g}_0,$$

where $K(t) : \mathfrak{g}^* \to \mathfrak{g}$ is a (time-varying) second-order-optimal symmetric gain operator satisfying the perturbed Riccati operator (7) given below,

$$\widehat{g}_0 = \arg\min_{g \in G} m_0(g),$$

and the residual $r_t(\widehat{g}) \in \mathfrak{g}^*$ is computed as

$$r_t(\widehat{g}) = T_e L^*_{\widehat{g}}[\big((D^{-1})^* \circ Q \circ D^{-1}(y - h_t(\widehat{g}))\big) \circ \mathrm{d}h_t(\widehat{g})].$$

The perturbed Riccati equation for K is

$$\begin{aligned} \dot{K} = &-c \cdot K + A \circ K + K \circ A^* - K \circ E \circ K \\ &+ B \circ R^{-1} \circ B^* - \omega_{Kr} \circ K - K \circ \omega^*_{Kr}, \end{aligned} \tag{7}$$

with initial condition $K(t_0) = X_0^{-1}$. The operators $X_0 : \mathfrak{g} \to \mathfrak{g}^*$, $A(t) : \mathfrak{g} \to \mathfrak{g}$, and $E(t) : \mathfrak{g} \to \mathfrak{g}^*$ are given by

$$\begin{aligned} X_0 &= T_e L^*_{\hat{g}_0} \circ \mathrm{Hess}\ m_0(\hat{g}) \circ T_e L_{\hat{g}_0}, \\ A(t) &= \mathrm{d}_1 \lambda_t(\hat{g}, u) \circ T_e L_{\hat{g}} - \mathrm{ad}_{\lambda_t(\hat{g},u)} - T_{\lambda_t(\hat{g},u)}, \\ E(t) &= -T_e L^*_{\hat{g}} \circ \big[\big((D^{-1})^* \circ Q \circ D^{-1}(y - h_t(\hat{g}))\big)^{T_{\hat{g}}G} \\ &\quad \circ \mathrm{Hess} h_t(\hat{g}) - (\mathrm{d}h_t(\hat{g}))^* \circ (D^{-1})^* \\ &\quad \circ Q \circ D^{-1} \circ \mathrm{d}h_t(\widehat{g})\big] \circ T_e L_{\hat{g}}. \end{aligned}$$

$T_e L_{\hat{g}}$ represents the tangent map of the left multiplication $L_{\hat{g}}$ applied at the identity e, $T^*_e L_{\hat{g}}$ its dual. ω features the connection function related to the choice of a left-invariant affine connection ∇ on the Lie group. $\mathrm{Hess} h_t(\hat{g})$ is the Hessian operator associated to the twice differentiable function h_t. $\mathrm{d}_1 \lambda(\widehat{g}, u)$ defines the differentials with respect to the first argument of the left trivialized dynamics. The adjoint operator satisfies $\mathrm{ad}_{\lambda_t(\hat{g},u)}(\cdot) = [\lambda_t(\hat{g}, u), \cdot]$, while $T_{\lambda_t(\hat{g},u)}$ represents the torsion function associated to the choice of the connection function. The symbol $\circ$ denotes the composition between maps, Kr is a shorthand notation for $K(t) r_t(\hat{g})$. R and Q are two symmetric positive definite matrices representative of the quadratic forms $\mathscr{R}$ and $\mathscr{Q}$, respectively.

IV. GEOMETRIC STRUCTURE

In order to apply the second-order filter to the system (1) it is necessary to investigate its geometric structure. The state space that underlies the kinematics (1) is the Lie group

$$G = \mathrm{SE}(2) \times \mathrm{SO}(2),$$

whose generic element $g \in G$ admits the matrix representation

$$g = \begin{bmatrix} \cos\alpha & -\sin\alpha & x & 0 & 0 \\ \sin\alpha & \cos\alpha & y & 0 & 0 \\ 0 & 0 & 1 & 0 & 0 \\ 0 & 0 & 0 & \cos\beta & -\sin\beta \\ 0 & 0 & 0 & \sin\beta & \cos\beta \end{bmatrix}.$$

Given the Lie algebra $\mathfrak{g} = \mathfrak{se}(2) \times \mathfrak{so}(2)$, we introduce the Lie algebra isomorphism $^\wedge : \mathbb{R}^4 \to \mathfrak{se}(2) \times \mathfrak{so}(2)$

$$\begin{bmatrix} \eta^x \\ \eta^y \\ \eta^\alpha \\ \eta^\beta \end{bmatrix}^\wedge \cong \begin{bmatrix} 0 & -\eta^\alpha & \eta^x & 0 & 0 \\ \eta^\alpha & 0 & \eta^y & 0 & 0 \\ 0 & 0 & 0 & 0 & 0 \\ 0 & 0 & 0 & 0 & -\eta^\beta \\ 0 & 0 & 0 & \eta^\beta & 0 \end{bmatrix},$$

from the Lie algebra $(\mathbb{R}^4, \star)$ to the matrix Lie algebra $(\mathfrak{se}(2), [\cdot,\cdot])$, where $\star : \mathbb{R}^3 \times \mathbb{R}^3 \to \mathbb{R}^3$ is the Lie bracket operation defined as

$$\begin{bmatrix} \eta_1^x \\ \eta_1^y \\ \eta_1^\alpha \\ \eta_1^\beta \end{bmatrix} \star \begin{bmatrix} \eta_2^x \\ \eta_2^y \\ \eta_2^\alpha \\ \eta_2^\beta \end{bmatrix} = \begin{bmatrix} -\eta_1^\alpha \eta_2^y + \eta_2^\alpha \eta_1^y \\ \eta_1^\alpha \eta_2^x - \eta_2^\alpha \eta_1^x \\ 0 \\ 0 \end{bmatrix},$$

and $[\cdot,\cdot]$ is the usual matrix commutator (see, e.g., [19]).

The left-trivialization dynamics of (1), obtained from $\lambda^\wedge = g^{-1}\dot{g}$, is given by $\lambda = (\lambda_x, \lambda_y, \lambda_\alpha, \lambda_\beta)$ where

$$\begin{aligned} \lambda_x &= V_1, \\ \lambda_y &= 0, \\ \lambda_\alpha &= \frac{1}{\ell_1} V_1 \tan\delta, \\ \lambda_\beta &= \frac{1}{\ell_2} V_1 \sin(\alpha - \beta) + \frac{\ell_{1_c}}{\ell_2} \frac{1}{\ell_1} V_1 \tan\delta \cos(\alpha - \beta). \end{aligned}$$

The tangent map and the adjoint representation are given by

$$\mathrm{T_e L_g} = \begin{bmatrix} \cos\alpha & -\sin\alpha & 0 & 0 \\ \sin\alpha & \cos\alpha & 0 & 0 \\ 0 & 0 & 1 & 0 \\ 0 & 0 & 0 & 1 \end{bmatrix},$$

$$\mathrm{ad}_{(\eta^\Omega)^\wedge} = \begin{bmatrix} 0 & -\eta^\alpha & \eta^y & 0 \\ \eta^\alpha & 0 & -\eta^x & 0 \\ 0 & 0 & 0 & 0 \\ 0 & 0 & 0 & 0 \end{bmatrix},$$

respectively.

We use the so-called Cartan-Schouten (0)-connection, characterized by $\omega^{(0)} = \frac{1}{2}\mathrm{ad}$, that has the following matrix representation

$$\omega^{(0)} = \frac{1}{2}\begin{bmatrix} 0 & -\eta^{\alpha} & \eta^{y} & 0 \\ \eta^{\alpha} & 0 & -\eta^{x} & 0 \\ 0 & 0 & 0 & 0 \\ 0 & 0 & 0 & 0 \end{bmatrix}.$$

This decision is justified by the fact that it has null torsion ([17]) and, in general, it results in better estimations.

The formulation of the geometric structure through matrices allows to simplify the treatment since all the compositions between the operators are carried out through matrix multiplications.

V. LABORATORY SETTING

The experimental validations were conducted on truck and semi-trailer scaled models at the Automotive Lab, Eindhoven University of Technology, within the project TruckLab. The operating space in the laboratory is $7\,\mathrm{m} \times 7\,\mathrm{m}$ including a docking station and tractors and semi-trailers. The laboratory is equipped with motion capture cameras Prime^{x}13 and, together with markers attached to the scaled vehicles, allows to have a position accuracy of about $\pm 20\,\mathrm{mm}$; so we can consider such measurements as the ground truth. The scaled vehicles operate on ROS (Robot Operating System) and are configured with Turtlebot3 Waffle Pi software architecture. The scaled model vehicles are a faithful reproduction of real truck semi-trailer vehicles, with a reduction ratio of 1:13.3. The model dimensions in Fig. 2 are listed in Table I.

parameter	scaled value [cm]	real value [m]
ℓ_1	28	3.72
ℓ_{1_c}	5.5	0.73
ℓ_2	56.7	7.54

TABLE I: Model datasheet.

The steering angle is measured with a combination of odometer and IMU measurements. The steering wheels of the scale reproductions have a maximum steering angle δ of $\pm 38\,\mathrm{deg}$. Thus, we impose the inequality $-38\,\mathrm{deg} \leq \delta \leq +38\,\mathrm{deg}$.

Another constraint is represented by the so-called jackknifing, that is a condition where the articulation angle between the tractor and the semi-trailer becomes very large. This problem can arise when driving forward and applying a large steering angle, or when driving backward (in this case the vehicle combination is unstable): a small constant steering input in the articulation angle will start to grow until the cabin collides with the semi-trailer. This condition results in the inequality $-100\,\mathrm{deg} \leq \gamma_1 \leq +100\,\mathrm{deg}$.

VI. SIMULATIONS

For the simulations, we consider two different measurement equations and apply them in two different moments of the parking maneuvering.

For the first part of the maneuver, when the truck is far away of the docking station, we assume to measure the position of two GPS devices settled in (x_0, y_0) and (x_2, y_2). Since the use of GPS is not sufficient during the maneuver that requires great precision (especially when reversing), we combine them with other sensors. In the second part of the maneuver, when the vehicle is sufficiently close to the final target, we simulate a LIDAR device settled at the docking station, to help the truck during the reverse (see Fig. 3). This LIDAR provides the pose of the trailer through a laser scan, in particular the position of (x_2, y_2) and the angle β. This is justified because, when reversing during the parking maneuver, the LIDAR can spot only the semi-trailer, and thus it can improve only its pose. Summarizing, the two measurement equations are the following:

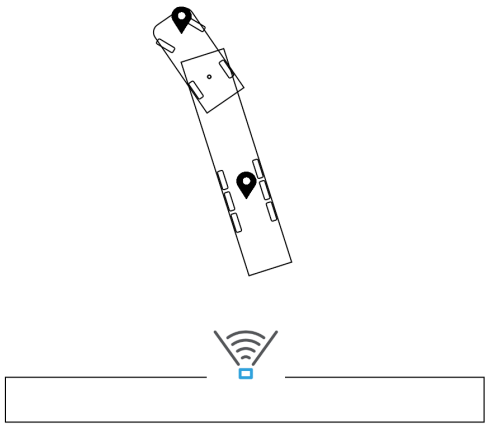

Fig. 3: LIDAR e GPS devices.

$$h_1(g(t),t) = \begin{bmatrix} x_{0_{\mathrm{GPS}}} \\ y_{0_{\mathrm{GPS}}} \\ x_{2_{\mathrm{GPS}}} \\ y_{2_{\mathrm{GPS}}} \end{bmatrix}, \quad h_2(g(t),t) = \begin{bmatrix} x_{0_{\mathrm{GPS}}} \\ y_{0_{\mathrm{GPS}}} \\ x_{2_{\mathrm{LIDAR}}} \\ y_{2_{\mathrm{LIDAR}}} \\ \beta_{\mathrm{LIDAR}} \end{bmatrix}.$$

To simulate noisy measurements given by these devices, we add Gaussian white noise to the reference trajectories provided by the optic cameras. The standard deviations of these measurement errors are reported in Table II.

measure	standard deviation
$x_{0_{\mathrm{GPS}}}$	5 m
$y_{0_{\mathrm{GPS}}}$	5 m
$x_{2_{\mathrm{GPS}}}$	5 m
$y_{2_{\mathrm{GPS}}}$	5 m
$x_{2_{\mathrm{LIDAR}}}$	0.10 m
$y_{2_{\mathrm{LIDAR}}}$	0.10 m
β_{LIDAR}	0.02 rad

TABLE II: Errors added to the real measurement to reduce the accuracy to behave like a real GPS system.

The linear velocity of the truck is obtained by adding to the scaled reference velocity a Gaussian white noise with a standard deviation of $0.1\mathrm{m/s}$.

The matrix representation of the quadratic forms $\mathscr{R}$, $\mathscr{Q}$ in (4) and of the linear operators B and D of (2) and (3) are

given by

$$R := \text{diag}\{1,1,1,1\}, \qquad B := \text{diag}\{0.1,0.1,0.1,0.1\},$$
$$Q := \text{diag}\{1,1,1,1\}, \qquad D := \text{diag}\{0.5,0.5,0.5,0.5\},$$

for the first filter, while for the second they are

$$R := \text{diag}\{1,1,1,1\}, \qquad B := \text{diag}\{0.1,0.1,0.1,0.1\},$$
$$Q := \text{diag}\{1,1,1,1,1\}, \quad D := \text{diag}\{0.5,0.5,0.5,0.5,0.5\}.$$

To solve the differential equations, we use a forward Euler method with a sample time of $T_s = 10$ms.

In Fig. 4a and Fig. 5a we show the maneuvers of the truck semi-trailer system for the two datasets. In Fig. 4b and 5b we report the reference and measured commands. In Fig. 4c and 5c we show the errors of the measured and filtered trajectories. The first vertical line corresponds to the instant when the vehicle starts the reverse maneuver, while the second one to the instant when the filter uses also the LIDAR sensor. As can be seen, the filter performs well even if the noises are large. When the vehicle starts the reverse maneuver the system becomes unstable. Consequently, the accuracy of the filter decreases, especially as far as it concerns the semi-trailer pose. The final errors due to filter approximation are acceptable if compared with the parking space, the dimension of the vehicles and the sensors' accuracy.

The addition of the LIDAR measurements significantly improves the precision of the filter and allows for better estimations in the final part of the maneuvering. Furthermore, a single LIDAR sensor can be installed directly on the docking station to reduce costs. For these purposes, also other laser scanner tools can be considered.

VII. CONCLUSION

In this paper we derived a second-order optimal minimum energy filter for a tractor semi-trailer system model. The laboratory and model simulated a scaled real case of a parking area where the trucks maneuver. To simulate GPS-like and LIDAR sensors, we added Gaussian white noises to the measurements obtained with an OptiTrack system. In the first part of the maneuver, when the truck is too far from the docking station, we consider two GPS-like devices settled at the midpoint of the front wheels of the truck and at the midpoint of the rear wheels of the semi-trailer. When the truck is maneuvering in reverse, close enough to the docking station, we added the more accurate measures of a LIDAR sensor.

The filter performs well in both driving parts of the scenario. Even if the errors of the GPS are large, compared with the maneuvering space, the filter produces good estimations of the state. The addition of the LIDAR allows to obtain an improvement of the measurements when the truck is approaching the station. The allowed error, in this case, should be as small as possible, since when reversing the control system becomes unstable and a small error in the estimation might cause big errors in the maneuvering. Moreover, the final parking target needs big precision to avoid causing damage to vehicles and structures.

For future works, we plan to insert the proposed filter in a controlled closed-loop system, to implement a sensor fusion between the measurements provided by GPS and LIDAR and to apply it to a real truck and semi-trailer vehicle system.

VIII. ACKNOWLEDGEMENTS

We are thankful to Viral Gosar, Ayush Maheshwari for the sharing of the datasets of the parking model and all the technical details of the scaled models and Erwin Meinders for his availability and help in the measurements of the laboratory settings. We are also grateful to Igo Besselink for the useful conversations on a reasonable choice of sensor configuration and their feedback on the work.

REFERENCES

[1] C. Samson, Control of chained systems application to path following and time-varying point-stabilization of mobile robots, IEEE transactions on Automatic Control 40 (1) (1995) 64–77.

[2] D. Tilbury, R. M. Murray, S. S. Sastry, Trajectory generation for the n-trailer problem using Goursat normal form, IEEE Transactions on Automatic Control 40 (5) (1995) 802–819.

[3] J. David, P. Manivannan, Control of truck-trailer mobile robots: a survey, Intelligent Service Robotics 7 (2014) 245–258.

[4] R. Quilez, A. Zeeman, N. Mitton, J. Vandaele, Docking autonomous robots in passive docks with infrared sensors and QR codes, EAI Endorsed Transactions on Self-Adaptive Systems 1 (2) (2015).

[5] L. Shen, P. R. Stopher, Review of GPS travel survey and GPS data-processing methods, Transport reviews 34 (3) (2014) 316–334.

[6] S. Ç. Tekkök, B. Bostanci, M. E. Söyünmez, O. Pınar, A Novel Docking Algorithm Based on the LiDAR and the V-shape Features, Avrupa Bilim ve Teknoloji Dergisi (26) (2021) 35–40.

[7] J. M. Esposito, M. Graves, An algorithm to identify docking locations for autonomous surface vessels from 3-D LiDAR scans, in: 2014 IEEE International Conference on Technologies for Practical Robot Applications (TePRA), IEEE, 2014, pp. 1–6.

[8] R. Kalman, A New Approach to Linear Filtering and Prediction Problems, ASME–Journal of Basic Engineering 82 (1) (1960) 35–45.

[9] B. D. Anderson, J. B. Moore, Optimal Filtering, Courier Corporation, 2012.

[10] A. Barrau, S. Bonnabel, The Invariant Extended Kalman Filter as a Stable Observer, IEEE Transactions on Automatic Control 62 (4) (2016) 1797–1812.

[11] A. Saccon, J. Trumpf, R. Mahony, A. P. Aguiar, Second-Order-Optimal Minimum-Energy Filters on Lie Groups, IEEE Transactions on Automatic Control 61 (10) (2015) 2906–2919.

[12] R. E. Mortensen, Maximum-Likelihood Recursive Nonlinear Filtering, Journal of Optimization Theory and Applications 2 (6) (1968) 386–394.

[13] D. Rigo, C. Segala, N. Sansonetto, R. Muradore, Second-Order-Optimal Filter on Lie Groups for Planar Rigid Bodies, IEEE Transactions on Automatic Control 67 (9) (2022) 4971–4977.

[14] D. Rigo, N. Sansonetto, R. Muradore, Second-order-optimal filtering on $SE(2)\times\mathbb{R}^2$ for the Chaplygin sleigh, Systems & Control Letters 178 (2023) 105568.

[15] D. Rigo, N. Sansonetto, R. Muradore, A comparison between the Extended Kalman Filter and a Minimum-Energy Filter in the TSE(2) case, in: 2021 60th IEEE Conference on Decision and Control (CDC), IEEE, 2021, pp. 6175–6180.

[16] F. Bullo, A. D. Lewis, Geometric Control of Mechanical Systems: Modeling, Analysis, and Design for Simple Mechanical Control Systems, Vol. 49, Springer, 2019.

[17] S. Kobayashi, K. Nomizu, Foundations of Differential Geometry, Vol. 1,2, New York, London, 1963.

[18] V. S. Varadarajan, Lie groups, Lie algebras, and Their Representations, Vol. 102, Springer Science & Business Media, 2013.

[19] J. E. Marsden, T. S. Ratiu, Introduction to Mechanics and Symmetry, Physics Today 48 (12) (1995) 65.

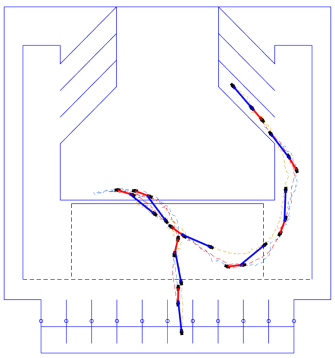

(a) Parking maneuver. With red and blue thick segments the truck and semi-trailer showed at regular intervals. With blue, red, and yellow dashed lines the reconstructed trajectories for the front wheels, rear wheels of the truck, and wheels of the semi-trailer, respectively.

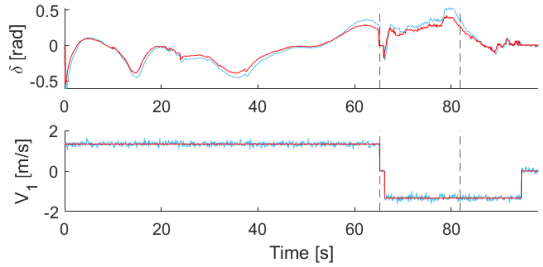

(b) Reference (red) and measured (light blue) commands.

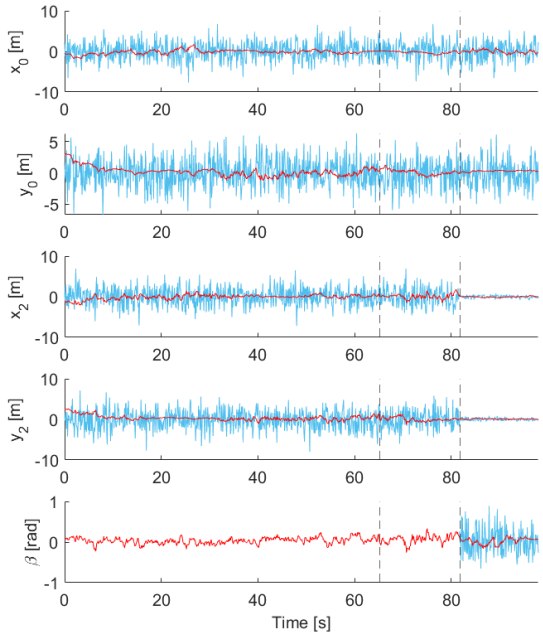

(c) Measured (light blue) and filtered (red) errors.

Fig. 4: Dataset 1.

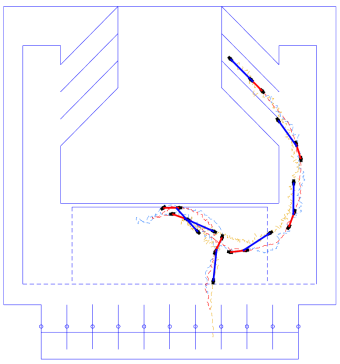

(a) Parking maneuver. With red and blue thick segments the truck and semi-trailer showed at regular intervals. With blue, red, and yellow dashed lines the reconstructed trajectories for the front wheels, rear wheels of the truck, and wheels of the semi-trailer, respectively.

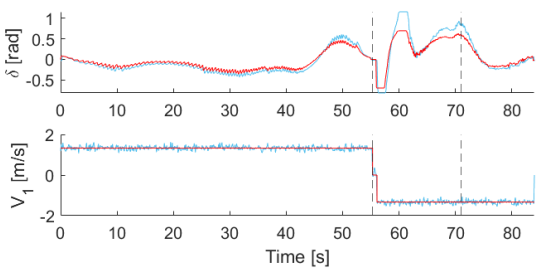

(b) Reference (red) and measured (light blue) commands.

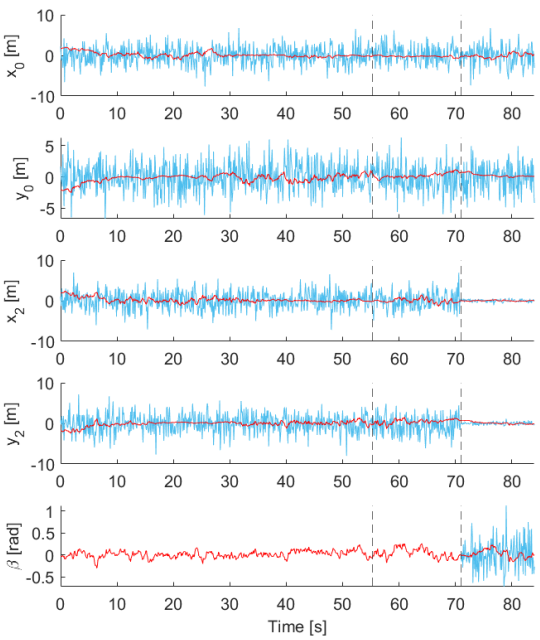

(c) Measured (light blue) and filtered (red) errors.

Fig. 5: Dataset 2.